Title

Chemo-mechanical Coupling in the Transport Cycle of a Type II ABC Transporter

Authors

Koichi Tamura[1*], Hiroshi Sugimoto[2,3], Yoshitsugu Shiro[2,3], Yuji Sugita[1,4,5]

[1] *Computational Biophysics Research Team, RIKEN Center for Computational Science, 6-7-1 Minatojima-Minamimachi, Chuo-ku, Kobe, Hyogo 650-0047, Japan*

[2] *Graduate School of Life Science, University of Hyogo, 3-2-1 Kouto, Kamigori, Ako, Hyogo 678-1297, Japan*

[3] *Synchrotron Radiation Life Science Instrumentation Team, RIKEN SPring-8 Center, 1-1-1 Kouto, Sayo, Hyogo 679-5148, Japan*

[4] *Theoretical Molecular Science Laboratory, RIKEN Cluster for Pioneering Research, 2-1 Hirosawa, Wako, Saitama 351-0198, Japan*

[5] *Laboratory for Biomolecular Function Simulation, RIKEN Center for Biosystems Dynamics Research, 6-7-1 Minatojima-Minamimachi, Chuo-ku, Kobe, Hyogo 650-0047, Japan*

* Corresponding author: k.tamur@gmail.com

ORCID IDs:

Koichi Tamura (0000-0002-9472-7555)

Hiroshi Sugimoto (0000-0002-3140-8362)

Yoshitsugu Shiro (0000-0003-0695-8327)

Yuji Sugita (0000-0001-9738-9216)

Abstract

ATP-binding cassette (ABC) transporters are integral membrane proteins that translocate a wide range of substrates across biological membranes, harnessing free energy from the binding and hydrolysis of ATP. To understand the mechanism of the inward- to outward-facing transition that could be achieved by tight regulation of ATPase activity through extensive conformational changes of the protein, we applied template-based iterative all-atom molecular dynamics (MD) simulation to the heme ABC transporter BhuUV-T. The simulations, together with biased MDs, predict two new conformations of the protein, namely, occluded (Occ) and outward-facing (OF) conformations. The comparison between the inward-facing crystal structure and the predicted two structures shows atomic details of the gating motions at the transmembrane helices and dimerization of the nucleotide-binding domains (NBDs). The MD simulations further reveal a novel role of the ABC signature motifs (LSGG[Q/E]) at the NBDs in decelerating ATPase activity in the Occ form through sporadic flipping of the side chains of the LSGG[Q/E] catalytic serine residues. The orientational changes are coupled to loose NBD dimerization in the Occ state, whereas they are blocked in the OF form where the NBDs are tightly dimerized. The chemo-mechanical coupling mechanism may apply to other types of ABC transporters having the conserved LSGG[Q/E] signature motifs.

Introduction

Chemo-mechanical couplings where large conformational changes of a protein are coupled to chemical events (i.e., binding and hydrolysis of nucleotide triphosphates) are often found in biomolecular motors,[1–3] signaling proteins,[3] chaperones,[4] and clock proteins.[5] The existence of the coupling implies that appropriate positioning[6] of the catalytically competent residues is realized only in a catalytic-dwell state of a protein and is disrupted in other conformational states of the cycle to prevent futile usage of ATP. For example, the formation of the catalytic-dwell state of the myosin motor is coupled to a global conformational change that brings the catalytic loop (switch II) closer to the ATP-binding P-loop.[7,8] Elucidation of chemo-mechanical coupling mechanism is central to understanding biomolecular machines including ATP-binding cassette (ABC) transporter.

ABC transporters are integral membrane proteins that are ubiquitous in all life forms and mediate the translocation of diverse substrates across the lipid bilayer, harnessing the free energy gained by the binding and hydrolysis of ATP.[9–11] They are involved in a vast variety of biological processes and their malfunction due to mutation often leads to serious medical conditions such as cystic fibrosis[12] and multidrug resistance.[13] Much attention has been paid to their transport mechanisms with a view to developing effective therapies.

ABC transporters have a common architecture: two transmembrane domains (TMDs) that form a substrate binding pocket, and two nucleotide-binding domains

(NBDs) that bind and hydrolyze ATP (Figure 1a). Some ABC transporters have covalently linked TMD and NBD, while in others the domains are separate. The TMDs and the NBDs are physically connected by coupling helices (CHs) which transmit the conformational change at the NBDs to the TMDs. Each NBD has a well-conserved[10,11] phosphate-binding motif (P-loop)[14] and an ABC signature motif (LSGG[Q/E]).[15] It is well established that the binding of ATP induces dimerization of the NBDs in a head-to-tail fashion in which the P-loop of one monomer sandwiches ATP with the signature motif of the opposite monomer (Figure 1b).[16,17] The dimerization realizes the formation of competent catalytic sites where the side chains of opposing monomers are oriented toward the substrate so that the transition state(s) of the hydrolysis reaction is stabilized.

The translocation of substrates by ABC transporters is thought to occur by an alternating access mechanism (Figure 1c).[10,11] In this mechanism, the structure of the ABC transporter alternates between inward-facing (IF) and outward-facing (OF) forms. The formation of an occluded (Occ) intermediate during the conformational transition between IF and OF makes the substrate binding pocket inaccessible to bulk solvent and prevents reverse transport. This is a key feature of transporters, and contrasts with channel proteins.

ABC transporters are classified into exporters and importers according to the substrate transport direction.[9] Importers, which are found only in prokaryotes, are further classified into type I, type II and energy coupling factor (ECF) transporters.[10,11] Each class of importer has a different substrate transport strategy and a specific

93 structural fold. Type I and II importers are associated with a periplasmic binding protein
94 (PBP) that binds substrate in the periplasm and delivers it to the TMDs of the ABC
95 transporter.[10,11] Type I importers transport relatively small compounds such as sugars,
96 while type II importers are specific for the transport of trace elements.[10,11] The ECF
97 transporters share a unique substrate acquisition mechanism and are devoted to the
98 transport of micronutrients.[18]

99 Atomic structures of full ABC transporters largely come from experimental
100 studies using X-ray crystallography[10,11] and/or cryo-electron microscopy.[19] These
101 techniques, however, often yield the protein structure of only one of the possible
102 conformational states and relatively unstable intermediates along the functional cycle
103 are difficult to elucidate, which is a major obstacle to the understanding of the coupling
104 mechanism. In this respect, atomistic molecular dynamics (MD) simulations are a
105 promising approach to reveal experimentally inaccessible conformational states in
106 transporters.[20–30] Homology (comparative) modeling techniques[31,32] are also widely
107 applied to predict elusive conformational states in a protein.[33,34] Since these techniques
108 do not take into account thermal motions of proteins, the conformational stability of
109 putative structures needs to be carefully examined by MD simulation.

110 In this study, we employ template-based iterative atomistic MD simulation to
111 predict hitherto unknown conformations of heme importer of *B. cenocepacia*
112 (BhuUV-T) [35] and provide insights into the mechanism of the IF-to-OF transition
113 occurring after substrate translocation. BhuUV-T belongs to the type II ABC importer
114 family and transports heme (Fe-porphyrin complex) across the inner membrane of

bacteria. Heme importers in pathogenic bacteria play a major role in the acquisition of iron, which is utilized during infection and propagation. BhuUV-T is a dimer of a dimer (BhuU (TMD) + BhuV (NBD)), together with a PBP (BhuT) (Figure 2a and S1). The coupling helices (CHs), which physically link the NBDs and the TMDs, are located between TM6 and 7 (Figure 2a and S1). BhuUV-T has been crystalized in an apo IF conformation with and without BhuT (throughout this manuscript, we use the term "apo" for the structure without bound nucleotides and substrates) and their structures have been characterized crystallographically.[35] The apo IF conformation with bound BhuT (Figure 2a) may represent a post-translocation state, in which a heme has already been released towards the cytoplasm. The transport cycle is postulated to proceed via the binding of ATP at the NBDs (BhuVs) to eventually form the OF state. The formation of the OF state would be accompanied by full dimerization of the NBDs (BhuVs) and the dissociation of BhuT. As mentioned, the cycle for transporters likely involves the transient formation of an Occ state after the translocation of substrate. Formation of the Occ state and closure of the cytoplasmic gate are thought to result from the binding of ATP and dimerization of the NBDs (BhuVs) (Figure 1c). The question which then arises is: how is the hydrolysis of ATP prevented in the Occ state, such that futile cycling back to the IF state is avoided, before formation of the OF state? To solve this problem, we analyzed MD trajectories of BhuUV-T starting from predicted Occ and OF conformations and arrived at a novel chemo-mechanical coupling mechanism that regulates ATPase activity by way of reorientation of the serine residues of the LSGG[Q/E] motifs in type II ABC transporters. The proposed mechanism likely

137 extends to other types of ABC transporters, as dimerization of NBDs is a common
138 feature.[10,11]
139

Computational Methods

Overall strategy. In this study, we focus on the IF-to-OF transition of heme importer BhuUV-T (Figure 2). Accordingly, our simulation systems do not contain the heme substrate. The unknown OF structure of the heme importer (Figure 2c) was modeled by template-based iterative MD simulation. The technique consists of iterative refinements of rough model by all atom MD simulations which consider solvent and membrane environment. The initial rough model was generated with homology modeling[31,32] using the structure of the vitamin B_{12} transport protein BtuCD in the ATP analog-bound form as template (PDB 4R9U).[36] Since 2002 several crystal structures of type II ABC importers have been elucidated, but the BtuCD structure is the only OF structure with bound nucleotides (Table S1). The engineered disulfide bond introduced in the BtuCD structure to suppress basal ATPase activity was not included in the homology model. The relatively low sequence identity (~34%) between BhuUV and BtuCD poses a significant challenge for homology modeling of thermally stable structures in the membrane environment. We therefore extensively refined the predicted structure by a series of MD simulations. Modeling procedures are briefly summarized in the following section, and details are described in SI (Text S1). The structural stabilities of the predicted structures were examined by relatively long (~1 μs) MD simulations without any restraints on protein atoms.

We first considered the nucleotide-bound Occ crystal structure of BtuCD-F (PDB 4FI3)[37] as a template of the Occ form, however, the lower resolution (3.47 Å) compared

to that of the OF form (2.79 Å) could have introduced further uncertainties into the modeling process. Instead, the Occ form (Figure 2b) was modeled by targeted MD (tMD) simulation[38] using part of the modeled OF structure as target (see below). The effect of the binding of ATP to the NBDs was then investigated by comparing the predicted structures with the crystal structure of the apo IF form (Figure 2). Representative MD simulations are summarized in Table S2.

Iterative refinements of the OF form. We employed MODELLER version 9.16 for building the homology models.[31,32] Sequence alignments were generated by the `align2d()` function in MODELLER, using the template 3D structure to put gaps in the alignment. For example, the function avoids placing gaps within the secondary structure. Altogether, we generated four structural models (MODEL1–4). The first OF model with bound ATP, which was based on an alignment involving several manual adjustments (MODEL1), turned out to be unstable after a short MD simulation of ~20 ns: we observed spontaneous closure of the periplasmic gate and distortion of the helices at Arg121 to Gly134 of both NBD monomers (Figure S2a and S2b). The instability, especially in the helical region in the NBDs, seemed to originate from the rather low sequence identity between BhuUV and the vitamin B_{12} transporter BtuCD used as template (Figure S2c). On the other hand, there is a crystal structure of a heme importer of *Y. pestis* (HmuUV) in the apo OF form (PDB 4G1U)[39] having a higher sequence identity (~40%) which can generate better models. Note that the *apo* HmuUV structure has a significantly different structural arrangement compared to that of the

184 *nucleotide-bound* BtuCD and therefore cannot be used as a template for the modeling of
185 the *nucleotide-bound* OF form of the *B. cenocepacia* heme importer BhuUV. As an
186 alternative, we generated a reference homology model (REF1) by using the apo
187 HmuUV structure as template and replaced the unstable regions in MODEL1 with the
188 corresponding ones of the REF1 structure to make a chimera. Although the helical
189 regions in the new model (MODEL2) turned out to be stable, some other parts were still
190 unstable: the periplasmic gate again spontaneously closed and there was disruption of
191 the dimer interface (data not shown). We speculated that the structural instability may
192 have arisen from the low sequence identity of TM6 connected to the CHs (Figure S1)
193 enlarging the dimer interface by way of the structural coupling. Then, we built the next
194 model (MODEL3), which involved replacing TM6 in MODEL2 with that in the REF1
195 structure. Although MODEL3 was stable during the first ~600 ns of the MD simulation,
196 the periplasmic gate gradually closed after this and eventually closed almost completely
197 (Figure S3a). We also observed fraying in the helical region at Ala51 to Ala70 in one of
198 the BhuU monomers (Figure S3b). The gradual closure of the periplasmic gate involved
199 TM5a of one monomer leaning towards the other (Figure S3a). Then, the final model,
200 MODEL4, was generated by replacing the fraying region and the leaning helix of
201 MODEL3 with the corresponding parts of the opposing monomer. This model turned
202 out to be stable during 1.5 μs MD simulation (MD-2ATP-OF) and, importantly, the
203 periplasmic gate stayed open (Figure S4a and S4b). C_α root mean squared deviation
204 (RMSD) between the template (PDB 4R9U) and the average structure of the predicted
205 OF form calculated from the last 500-ns part of the MD trajectory was 2.2 Å (Figure

206 S4c). More details of the modeling are found in SI.

207

208 **Modeling of the Occ intermediate.** Targeted MD (tMD) simulation[38] starting from
209 the equilibrated ATP-bound IF structure was employed to model an Occ conformation
210 of BhuUV-T with bound nucleotides. tMD has been widely used to elucidate the
211 conformational transition pathways of proteins including a type II ABC transporter.[40] In
212 tMD, a biasing force is applied to pull the protein towards a predefined target structure.
213 The application of the external force enables one to induce conformational changes in
214 proteins very efficiently. A caveat is that this method is known to be subject to
215 "large-scales-first" bias and the pathway may deviate from the actual physical one.[41,42]
216 We thus disregarded the pathway itself and checked only for stability in the final model.
217 Note that if one chooses the entire MODEL4 OF structure as a target of tMD, the
218 simulation would end up with generating the target structure itself. Alternatively, if one
219 selects a part of the MODEL4 structure as a target, one would obtain protein with the
220 selected part having conformation of the MODEL4 and the remaining part left almost
221 unaffected. In our case, the NBDs and the residues of the cytoplasmic gate of the
222 equilibrated ATP-bound IF structure were pulled so that the domains and the gate closed
223 as in the MODEL4 OF structure (see SI for details). We then performed an equilibrium
224 MD simulation without the bias potential on the protein atoms to check the structural
225 stability of the predicted Occ form. However, this first model was unstable: there was
226 immediate opening of the cytoplasmic gate and widening of the distances between
227 coupling helices in a short MD simulation (data not shown). Then, a second model was

generated by also pulling TM6 and 7 of both monomers towards the target (MODEL4). An equilibrium MD simulation (1.5 μs) confirmed the structural stability of the predicted Occ form (MD-2ATP-Occ, Figure S5a). C_α-RMSD between the averaged structure along the last 500-ns part of the MD trajectory of the Occ form and the BtuCD-F Occ crystallographic one was 2.5 Å (Figure S5b).

MD Simulation details. All MD simulations were performed with the development version of GENESIS.[43,44] The force field parameter set for water molecules was TIP3P,[45,46] and those for protein and lipids were CHARMM36.[47,48] We used revised parameters for ATP[49] and magnesium ions.[50] The protein was embedded in a 1-palmitoyl-2-oleoyl-sn-glycero-3-phosphoethanolamine (POPE) bilayer. Typical simulation system size was 134 × 134 × 197 $Å^3$ (~360,000 atoms) for the BhuUV-T system and 134 × 134 × 154 $Å^3$ (~280,000 atoms) for the BhuUV system. The equation of motion was integrated with the velocity Verlet algorithm with a time step of 2.5 fs. Bonds including a hydrogen atom were constrained by the SHAKE/RATTLE[51] (non-water molecules) and the SETTLE[52] (water molecules) algorithms. Temperature and pressure were regulated by the stochastic velocity rescaling thermostat[53] and the barostat,[54] respectively. The thermostat and the semi-isotropically coupled barostat were applied every 10 steps. Long range electrostatic interactions were calculated with the particle mesh Ewald method[55] and updated every 2 steps. Short range Lennard-Jones interactions were cutoff at 12 Å with a force switching function beginning at 10 Å.[56] Details are described in SI. MD trajectories related with the manuscript are available at

this link https://osf.io/hfb2c/.

Results

Characteristics of the Predicted Occ and OF Structures.

Crystal structures of heme importer BhuUV and vitamin B_{12} transporter BtuCD have identified two gates for heme transport, i.e., the cytoplasmic gate and the periplasmic gate. The cytoplasmic gate, especially the so-called cytoplasmic gate II, is formed by Asn108 and Leu110 (numbering of BhuUV) of opposing monomers which are well conserved among type II ABC transporters (Figure 3a).[37] The periplasmic gate of BhuUV(-T) is formed by Asp200 and Arg204 of opposite subunits which are conserved among heme importers (Figure 4, left).[35] In the IF state of the BhuUV-T crystal structures, the cytoplasmic gate II is widely opened, while the periplasmic gate is closed through a salt bridge between Asp200 and Arg204 (Figure 3a and Figure 4, left).[35] Eventually, the PBP BhuT stably associates to the periplasmic surface of TMD of BhuUV through the electrostatic interaction of Glu94 or Glu231 (BhuT) and Arg84 (BhuU) (Figure S6).[35] In the MD simulations of the IF and Occ states, however, those salt-bridges were disrupted, and instead salt-bridge pairs between Glu94 or Glu231 and Arg81 (Bhu) were formed (Figure S5c and S6).

In our predicted Occ structures of BhuUV-T, both gates are closed and BhuT still binds to TMD (Figure 3b and 4, middle). In addition, the central cavity, although large enough to accommodate the substrate heme, is filled with water molecules (Figure S7a). The predicted Occ structural characteristics fit well with the crystal structure of the Occ state of the BtuCD-F complex with bound ATP analogs (PDB 4FI3), in which a large

central cavity for substrate is also observed (Figure S7b).[37] On the other hand, in the predicted OF structure of BhuUV, the periplasimic gate is opened, while the cytoplasmic gate II is closed (Figure 3c and 4, right). Details of the conformational change from IF to the unique Occ conformation found in our simulation are described in the following section.

Differences between the predicted OF and Occ forms of BhuUV(-T) and the crystal structures of BtuCD (PDB 4R9U)[36] and BtuCD-F (PDB 4FI3)[37] are best characterized by the distance between the coupling helices (CHs). The distance in both predicted structures is shorter (~2–4 Å) than that in the corresponding crystal structures (Figure 5). A shorter distance causes a greater tilt of TM6 and 7 of opposing monomers (Figure S8), and the strong tilt of the TM helices, especially in the OF form, stabilizes an open periplasmic gate. However, in the MD simulation of the ATP-bound OF BtuCD with the engineered disulfide bond (BtuCD-2ATP-OF) there is spontaneous closure of the periplasmic gate within a short period (Figure S9). Spontaneous closure was often observed in the simulation of the apo OF BtuCD (PDB 1L7V) whose periplasmic gate is structurally similar to that of the ATP-bound form (PDB 4R9U).[20,57,58] In contrast, the simulation of the predicted OF form of BhuUV finds a state in which the periplasmic gate is stably opened due to a greater tilt of the TM helices in the membrane environment (Figure S4b). Therefore, the modeled structures of BhuUV-T are likely more relevant to physiological conditions, while the BtuCD(-F) crystal structures seem trapped in slightly unnatural states possibly due to the introduction of the artificial disulfide bond and the mutations. Indeed, the mutated BtuCD proteins did not exhibit

297 ATP hydrolysis activity.[37]

298

299 **NBD Dimerization Induces Closure of Cytoplasmic Gate and Opening of**
300 **Periplasmic gate.**

301 The opened cytoplasmic gate II in the IF structure is due directly to separation of the
302 extended stretch (exTM3) of opposing monomers (Figure 3a). In the initial step from
303 the IF state to the Occ state, the binding of ATP promotes dimerization of the NBDs
304 (Figure 3a, ①), and eventually forces the coupling helices (CHs) and the TM6/7
305 bundles to lean towards the central cavity (Figure 3a, ②). These conformational
306 changes pushes TM2, and forces its C-terminal part to tilt towards the central cavity,
307 eventually closing the cytoplasmic gate II bordered by the exTM3s (Figure 3b). Tight
308 closure of the gate was maintained throughout the MD simulations of the Occ state
309 (Figure S5d) and of the OF state (Figure S4d).

310 The disposition of the periplasmic gate of BhuUV(-T) in the IF crystal structure
311 persists in the predicted Occ state despite large conformational changes in the NBDs
312 and several TM helices (Figure 4, middle, and Figure S5e). On the other hand, in the OF
313 state, the periplasmic gate is opened due to the tilt of TM5 and 5a together with other
314 helices (Figure 4, right, and Figure S4b). The large tilt of the helices on the periplasmic
315 side of the TMD is coupled to the dissociation of BhuT from TMD BhuU, as discussed
316 later. Gate opening and closing is highly correlated with dimerization of the NBD. We
317 measured the distance between two CHs from each NBD monomer for the IF, Occ and
318 OF structures. As shown in Figure 5, the average distance is 37.1, 30.0 and 26.4 Å, in

the MD simulation of the IF, Occ and OF states, respectively. The dimerized forms of Occ and OF states are somewhat different. The inter-NBD distance of the Occ form gradually increases and deviated from that of the OF form (Figure S10). We defined the NBD structure of Occ and OF as "partial" and "full" dimerization forms, respectively.

Stoichiometry of ATP in the IF-to-OF transition of BhuUV-T.

The role of bound ATP in closing the cytoplasmic gate II was examined in a series of MD simulations. In the predicted Occ and OF forms of BhuUV(-T), two ATPs are tightly bound to the active sites and contribute to the tight closure of cytoplasmic gate II (Figure 3). This is similar to what is observed in the corresponding crystal structures of BtuCD(-F).[36,37] Consistently, when we added two ATPs to the NBDs of the apo IF BhuUV-T complex, the CHs, which directly contact the NBDs, tended move closer (Figure 6a). The importance of ATPs is further highlighted by the following observation: when we removed two ATPs from the predicted Occ state, there was spontaneous widening of the CH distance (Figure 6a). Importantly, the narrowing and widening of the CH distance clearly correlates with the tendency to formation and destabilization of the cytoplasmic gate II, respectively (Figure 6b), demonstrating mechanical coupling between the NBD and the TMD. Destabilization of the dimer interface upon removal of ATPs is also seen in the BtuCD-F system.[59]

Is *one* ATP enough to stably close cytoplasmic gate II? To answer this, we removed one ATP from an arbitrarily chosen active site of the predicted Occ form. Although the result was not so as clear as in the simulations above, the distance between

the CHs consistently widened (Figure 6a). The widening transiently opens the cytoplasmic gate (Figure 6b). These results suggest that one ATP may be insufficient to stably close the cytoplasmic gate, and a longer simulation may clarify this.

Dissociation of the PBP from TMD Facilitates NBD Dimerization.

In the MD simulation of the predicted Occ form with bound ATP, BhuT was stably bound to the TMDs, as shown by the distance between conserved[35] salt-bridge pairs between the TMDs and BhuT (Figure S5c). The observation seems inconsistent with our previous pull-down assays performed on BhuUV-T, which show that the binding of ATP, not its hydrolysis, induces dissociation of BhuT.[35] Therefore, the Occ form appears to be in a BhuT-dissociation dwell state with a longer dwelling time than the simulation time scale (1.5 μs).

A comparison between Occ and OF structures showed that the CHs and the helix bundles (TM6/7) in the OF form lean further than those in the Occ form, resulting in the opening the periplasmic gate (Figure 4 and 5). However, these structural changes could not be allowed in the BhuUV-T Occ form, probably due to the capping by the bound BhuT. Therefore, it was indicated that the dissociation of BhuT (PBP) from TMD of BhuUV and the structural change on the periplasmic side are coupled with each other, which is followed by "full" dimerization of the NBDs (Figure 2c). In other words, PBP (BhuT) dissociation facilitates NBD (BhuV) dimerization.

Orientation of the Catalytic Serine Residues.

363 During MD simulation of the Occ state, we witnessed orientational changes of the
364 catalytically important serine residues (Ser147)[60] in the LSGG[Q/E] motifs in the NBDs
365 (Figure 7a, upper panel). Namely, the side chain of Ser147 in either monomer
366 occasionally flipped between the γ-phosphate of ATP and the glutamate residue of the
367 LSGG[Q/E] motif (Figures 7a, 7c and S11a). The change in orientation from the
368 potentially catalytic to the non-catalytic forms clearly correlates with a subtle increase
369 in the distance between the P-loop and the LSGG[Q/E] motif (Figure 7a) which
370 sandwich ATP (Figure 7c), due to the "partial" dimerization.

371 As shown in Figure 7a, an interesting finding in the Occ state is that the side chain
372 swiveling occurred more frequently in one of the nucleotide-binding sites than the other.
373 Here, we designate the former as NBS1 and the latter as NBS2, respectively. The
374 difference in side-chain mobility of Ser147 originates from the asymmetrical
375 dimerization in the Occ state. The distance between the P-loop and the LSGG[Q/E]
376 motif in NBS1 is larger than that in NBS2, resulting in more frequent dissociation of the
377 side chain of the serine residue (Figure 7a, lower panel).

378 In contrast, in the OF state, Ser147 of both monomers is always perfectly oriented
379 toward the γ-phosphate of ATP (Figure 7b, upper panel) presumably due to the stable
380 "full" dimerization of the NBDs (Figure 7b, lower panel and Figure S10). The "full"
381 dimerization (Figure S10) realizes shorter distances and holds the serine residues in a
382 catalytic orientation (Figure 7b). Ser147 appears key in modulating the catalytic power
383 of the protein in the functional cycle, as discussed below.

384

385

Discussion and Conclusions

In this study, we predicted two unknown conformations of a type II heme ABC importer BhuUV-T in order to elucidate the mechanism by which the futile usage of ATP in the Occ state can be avoided. The results lead us to propose a chemo-mechanical coupling mechanism where the Ser residues (Ser147) of the ABC signature LSGG[Q/E] motifs play a fundamental role in modulating catalytic activity of the transporter (Figure 8). In this mechanism, the progress of conformational changes of the protein determines ATPase activity, in the following manner:

1. In the IF state, the protein is in an ATP-binding dwell and the catalytic sites are "empty" (without bound ATP), as represented by the crystal structure (PDB 5B58).

2. The binding of ATP to NBD (BhuV) of the IF form triggers a conformational change to the Occ form. The Occ form is apparently in a BhuT-dissociation dwell, because the bound BhuT hinders further tilting of TM helices and narrowing of the inter-CHs space. The structural constraint holds the NBDs somewhat apart due to structural coupling between the NBDs and the CHs, stabilizing "partial" dimerization. As a result, the catalytic sites are in a "loose" state, in which the Ser residues (Ser147) of LSGG[Q/E] motifs frequently flip away from the γ-phosphate of ATP, and thereby catalytic activity is partially lost. The hydrolysis reaction is decelerated.

3. In going from the Occ to OF states, dimerization of the NBDs gradually proceeds, and with the dissociation of BhuT full tilting of the TM helices and complete dimerization of the NBDs are achieved. These conformational changes gradually

408 constraint the side chains of the two Ser147s so that their orientations become
409 increasingly catalytic and full competency and maximal ATPase activity are realized
410 upon final dimer engagement of the NBDs. These catalytic sites are now in a "tight"
411 state (Figure 8).

412 Oldham and Chen[61] have recently pointed out the role of the serine residues in
413 coupling conformational change of a type I maltose ABC transporter to its catalytic
414 activity, and that its role resembles that of the "arginine finger" of the biomolecular
415 motor F_1-ATPase, which controls the catalytic activity of the protein.[62] However, to our
416 knowledge, the mechanism, by which the wasteful hydrolysis of ATP in the Occ state is
417 avoided, has not yet been addressed for any ABC transporters. Here, by combined use
418 of structural modeling and MD simulation, the mechanism of chemo-mechanical
419 coupling in the type II ABC transporter can be explained in atomistic detail.

420 With respect to the mechanism of the heme transport by BhuUV-T, our
421 mechanism proposed for BhuUV-T is apparently similar to that for the molybdate
422 importer MolBC, but somewhat different from those for BtuCD-F and HmuUV.[11,37,63–66]
423 For example, the closure of the cytoplasmic gate II in the proposed IF-to-OF transition
424 pathway of BhuUV-T is consistent with an electron paramagnetic resonance (EPR)
425 spectroscopy study on MolBC.[63] Moreover, key features in the crystal structure of
426 MolBC are consistent with those of BhuUV. Both structures have been determined in
427 the IF form without bound ATP.[35,64] On the other hand, the existing crystal structures of
428 BtuCD and HmuUV without bound ATP were solved in the OF form with a closed
429 cytoplasmic gate I, which is bordered by the N-terminal part of TM5 of opposing

monomers (Table S1).

The transport cycle of a vitamin B_{12} transporter BtuCD-F of type II ABC importer family involves a different state that is not considered in this study.[11,37] Namely, the ATP-binding dwell of BtuCD-F is an asymmetric apo Occ state (PDB 2QI9),[65] unlike to BhuUV-T and MolBC (Figure S12a). Notably, the cytoplasmic side of the asymmetric apo Occ crystal structure is closed differently from BhuUV-T and MolBC. The gate of BtuCD-F in the apo Occ state is at cytoplasmic gate I. Furthermore, the transport cycle of BtuCD-F does not involve a state like the PBP-dissociation dwell (Figure S12b, middle), even though a crystal structure that could represent the state has been found for BtuCD-F (PDB 4FI3, Figure S12a). Alternatively, this latter BtuCD-F structure has been considered to be a vitamin B_{12}-loaded Occ state despite the absence of bound substrate in the crystal structure.[11,37] These studies imply some mechanistic divergence among the type II ABC importer family, a view supported by a recent biochemical study on HmuUV.[66]

It seems that the binding of ATP to the NBDs of the asymmetric Occ form of BtuCD-F inevitably forces dimerization of the NBDs, resulting in opening of the cytoplasmic gate I and closure of cytoplasmic gate II, as observed in the crystal structure (PDB 4FI3). Therefore, the ATP-bound form of the Occ state with the cytoplasmic gate II closed may appear between the asymmetric occluded and the OF forms, as proposed in the transport mechanism of BhuUV-T (Figure 8 and S12b). Concern over a futile hydrolysis reaction in the ATP-bound Occ form can be partially allayed by our chemo-mechanical coupling mechanism.

The dynamic nature of ABC transporters renders experimental elucidation of chemo-mechanical coupling mechanisms a challenging task. For instance, ATPase activity of BhuUV-T is measured as the time course of the concentration of released inorganic phosphate ions upon the addition of ATP.[35] The observed kinetic parameters represent multiple dynamic processes including the IF-to-OF conformational transition and the dissociation of BhuT, complicating interpretation. The complexity behind such a single experimental parameter highlights the usefulness of our coupled computational structural modeling and MD simulation approach in deciphering chemo-mechanical coupling, as it allows for direct characterization of motions of a protein and its catalytic sites along the functional cycle. The prediction from simulation and our proposed mechanism can now be tested experimentally.

In summary, template-based iterative MD simulation and biased MD predict two structurally unknown conformations of type II heme ABC importer BhuUV-T, and provide insights into the chemo-mechanical coupling mechanism. Both structures exhibit high stability in a membrane environment and show how binding of ATP is coupled to conformational changes of the protein. The dimerization of the NBDs in the predicted Occ form is incomplete due to structural constraints imposed by bound BhuT. As a consequence, the side chains of the serine residues of the conserved LSGG[Q/E] motifs flip between catalytic and non-catalytic orientations, resulting in impaired catalytic activity. Dissociation of BhuT in the OF form enable tight dimerization of the NBDs and proper serine orientation, activating full catalytic power of the protein. These results led us to a definitive answer to the question on the futile usage of ATP in the Occ

474 state. The proposed chemo-mechanical coupling mechanism may provide basis for the
475 understanding of transport mechanism of many ABC transporters having different
476 structural folds.

Acknowledgments

K.T. thanks J. Jung, C. Kobayashi, Y. Matsunaga, and M. Kamiya for sharing their expertise on running simulations on the K computer. This work was supported by the RIKEN pioneering project "Dynamic Structural Biology" (to Y.Sugita), MEXT Grant-in-Aid for Scientific Research on Innovative Areas Grant Number 26119006 (to Y.Sugita), JP26220807 (to Y.Shiro), JP15H01655, JP17H05896 (to H.Sugimoto), and RIKEN Special Postdoctoral Researcher Program (to K.T.). This research used computational resources of the K computer provided by the RIKEN Center for Computational Science through the HPCI System Research project (to K.T., Project ID: hp170027, hp180009, to Y.Sugita, ra000009). Molecular figures were prepared with VMD[67] and PyMOL.[68]

References

1. R Watanabe and H Noji, 2013, Chemomechanical coupling mechanism of F_1-ATPase: Catalysis and torque generation, *FEBS Lett.*, **587**: 1030–1035.
2. M Preller and DJ Manstein, 2013, Myosin structure, allostery, and mechano-chemistry, *Structure*, **21**: 1911–1922.
3. MP Mueller and RS Goody, 2016, Ras GTPases and myosin: qualitative conservation and quantitative diversification in signal and energy transduction, *Biopolymers*, **105**: 422–430.
4. LH Pearl and C Prodromou, 2006, Structure and mechanism of the Hsp90 molecular chaperone machinery, *Annu. Rev. Biochem.*, **75**: 271–294.
5. J Abe, TB Hiyama, A Mukaiyama, S Son, T Mori, S Saito, M Osako, J Wolanin, E Yamashita, T Kondo, and S Akiyama, 2015, Atomic-scale origins of slowness in the cyanobacterial circadian clock, *Science*, **349**: 312–316.
6. A Warshel, 1998, Electrostatic origin of the catalytic power of enzymes and the role of preorganized active sites, *J. Biol. Chem.*, **273**: 27035–27038.
7. S Koppole, JC Smith, and S Fischer, 2007, The structural coupling between ATPase activation and recovery stroke in the myosin II motor, *Structure*, **15**: 825–837.
8. Y Yang, H Yu, and Q Cui, 2008, Extensive conformational transitions are required to turn on ATP hydrolysis in myosin, *J. Mol. Biol.*, **381**: 1407–1420.
9. IB Holland and MA Blight, 1999, ABC-ATPases, adaptable energy generators fueling transmembrane movement of a variety of molecules in organisms from bacteria to humans, *J. Mol. Biol.*, **293**: 381–399.
10. J ter Beek, A Guskov, and DJ Slotboom, 2014, Structural diversity of ABC transporters, *J. Gen. Physiol.*, **143**: 419–435.
11. KP Locher, 2016, Mechanistic diversity in ATP-binding cassette (ABC) transporters, *Nat. Struct. Mol. Biol.*, **23**: 487–493.
12. T-C Hwang, J-T Yeh, J Zhang, Y-C Yu, H-I Yeh, and S Destefano, 2018, Structural mechanisms of CFTR function and dysfunction, *J. Gen. Physiol.*, **150**: 539–570.
13. RW Robey, KM Pluchino, MD Hall, AT Fojo, SE Bates and MM Gottesman, 2018, Revisiting the role of ABC transporters in multidrug-resistance cancer, *Nat. Rev. Cancer*, **18**: 452–464.
14. JE Walker, M Saraste, MJ Runswick, and NJ Gay, 1982, Distantly related

sqquences in the α- and β-subunits of ATP synthase, myosin, kinases and other ATP-requiring enzymes and a common nucleotide binding fold, *EMBO J.*, **1**: 945–951.

15. CH Higgins, ID Hiles, GPC Salmond, DR Gill, JA Downie, IJ Evans, IB Holland, L Gray, SD Buckel, AW Bell, and MA Hermodson, 1986, A family of related ATP-binding subunits coupled to many distinct biological processes in bacteria, *Nature*, **323**: 448–450.
16. PM Jones and AM George, 1999, Subunit interactions in ABC transporters: towards a functional architecture, *FEMS Microbiol. Lett.*, **179**: 187–202.
17. PC Smith, N Karpowich, L Millen, JE Moody, J Rosen, PJ Thomas, and JF Hunt, 2002, ATP binding to the motor domain from an ABC transpoter drives formation of a nucleotide sandwich dimer, *Mol. Cell.*, **10**: 139–149.
18. P Zhang, 2013, Structure and mechanism of energy-coupling factor transporters, *Trends Microbiol.*, **21**: 652–659.
19. J-Y Lee and DE Rosenbaum, 2017, Transporters revealed, *Cell*, **168**: 951–953.
20. J Sonne, C Kandt, GH Peters, FY Hansen, MO Jensen, and DP Tieleman, 2007, Simulation of the coupling between nucleotide binding and transmembrane domains in the ATP binding cassette transporter BtuCD, *Biophys. J.*, **92**: 2727–2734.
21. PY Pendse, BR Brooks, and JB Klauda, 2010, Probing the periplasmic-open state of lactose permease in response to sugar binding and proton translocation, *J. Mol. Biol.*, **404**: 506–521.
22. SA Shaikh and E Tajkhorshid, 2010, Modeling and dynamics of the inward-facing state of a Na^+/Cl^- dependent neurotransmitter transporter homologue, *PLoS Comput. Biol.*, **6**: e1000905.
23. M Moradi and E Tajkhorshid, 2013, Mechanistic picture for conformational transition of a membrane transporter at atomic resolution, *Proc. Natl. Acad. Sci. USA*, **110**: 18916–18921.
24. J-P Machtens, D Kortzak, C Lansche, A Leinenweber, P Kilian, B Begemann, U Zachariae, D Ewers, BL de Groot, R Briones, and C Fahlke, 2015, Mechanisms of anion conduction by coupled glutamate transporters, *Cell*, **160**: 542–553.
25. M Moradi, G Enkavi and E Tajkhorshid, 2015, Atomic-level characterization of transport cycle thermodynamics in the glycerol-3-phosphate:phosphate antiporter,

Nat. Commun., **6**: 8393.

26. MH Cheng and I Bahar, 2015, Molecluar mechanism of dopamine transport by human dopamine transporter, *Structure*, **23**: 2171–2181.
27. A Pietropaolo, CL Pierri, F Palmieri, and M Klingenberg, 2016, The switching mechanism of the mitochondrial ADP/ATP carrier explored by free-energy landscapes, *Biochim. Biophys. Acta*, **1857**: 772–781.
28. K Tamura and S Hayashi, 2017, Atomistic modeling of alternating access of a mitochondrial ADP/ATP membrane transporter with molecular simulations, *PLoS ONE*, **12**: e0181489.
29. M Ke, Y Yuan, X Jiang, Nieng Yan, and H Gong, 2017, Molecular determinants for the thermodynamic and functional divergence of uniporter GLUT1 and proton symporter XylE, *PLoS Comput. Biol.*, **13**: e1005603.
30. H Goddeke, MH Timachi, CAJ Hutter, L Galazzo, MA Seeger, M Karttunen, E Bordignon, and LV Schafer, 2018, Atomistic mechanism of large-scale conformational transition in a heterodimeric ABC exporter, *J. Am. Chem. Soc.*, **140**: 4543–4551.
31. A Sali and TL Blundell, 1993, Comparative protein modelling by satisfaction of spatial restraints, *J. Mol. Biol.*, **234**: 779–815.
32. MA Marti-Renom, AC Stuart, A Fiser, R Sanchez, F Melo, and A Sali, 2000, Comparative protein structure modeling of genes and genomes, *Annu. Rev. Biophys. Biomol. Struct.*, **29**: 291–325.
33. L Domicevica and PC Biggin, 2015, Homology modelling of human P-glycoprotein, *Biochem. Soc. Trans.*, **43**: 952–958.
34. I Callebaut, B Hoffmann, P Lehn, and J-P Mornon, 2017, Molecular modeling and molecular dynamics of CFTR, *Cell. Mol. Life. Sci.*, **74**: 3–22.
35. Y Naoe, N Nakamura, A Doi, M Sawabe, H Nakamura, Y Shiro, and H Sugimoto, 2016, Crystal structure of bacterial haem importer complex in the inward-facing conformation, *Nat. Commun.*, **7**: 13411.
36. VM Korkhov, SA Mireku, DB Veprintsev, and KP Locher, 2014, Structure of AMP-PNP-bound BtuCD and mechanism of ATP-powered vitamin B12 transport by BtuCD-F, *Nat. Struct. Mol. Biol.*, **21**: 1097–1099.
37. VM Korkhov, SA Mireku, and KP Locher, 2012, Structure of AMP-PNP-bound vitamin B_{12} transporter BtuCD-F, *Nature*, **490**: 367–372.

38. J Schlitter, M Engels, P Krüger, E Jacoby and A Wollmer, 1993, Targeted molecular dynamics simulation of conformational change-application to the T ↔ R transition in insulin, *Mol. Simul.*, **10**: 291–308.
39. J-S Woo, A Zeltina, BA Goetz and KP Locher, 2012, X-ray structure of the *Yersinia pestis* heme transporter HmuUV, *Nat. Struct. Mol. Biol.*, **19**: 1310–1315.
40. J Weng, K Fan, and W Wang, 2012, The conformational transition pathways of ATP-binding cassette transporter BtuCD revealed by targeted molecular dynamics simulation, *PLoS ONE*, **7**: e30465.
41. V Ovchinnikov and M Karplus, 2012, Analysis and elimination of a bias in targeted molecular dynamics simulations of conformational transitions: application to calmodulin, *J. Phys. Chem. B*, **116**: 8584–8603.
42. K Tamura and S Hayashi, 2015, Linear response path following: a molecular dynamics method to simulate global conformational changes of protein upon ligand binding, *J. Chem. Theory Comput.*, **11**: 2900–2917.
43. J Jung, T Mori, C Kobayashi, Y Matsunaga, T Yoda, M Feig, and Y Sugita, 2015, GENESIS: A hybrid-parallel and multi-scale molecular dynamics simulator with enhanced sampling algorithms for biomolecular and cellular simulations, *WIREs Comput. Mol. Sci.*, **5**: 310–323.
44. C Kobayashi, J Jung, Y Matsunaga, T Mori, T Ando, K Tamura, M Kamiya, and Y Sugita, 2017, GENESIS 1.1: A hybrid-parallel molecular dynamics simulator with enhanced sampling algorithms on multiple computational platforms, *J. Comput. Chem.*, **38**: 2193–2206.
45. AD MacKerell, D Bashford, M Bellott, RL Dunbrack, JD Evanseck, MJ Field, et al., 1998, All-atom empirical potential for molecular modeling and dynamics studies of proteins, *J. Phys. Chem. B*, **102**: 3586–3616.
46. WL Jorgensen, J Chandrasekhar, JD Madura, RW Impey, and ML Klein, 1983, Comparison of simple potential functions for simulating liquid water, *J. Chem. Phys.*, **79**: 926–935.
47. RB Best, X Zhu, J Shim, PEM Lopes, J Mittal, M Feig, and AD Mackerell, Jr., 2012, Optimization of the additive CHARMM all-atom protein force field targeting improved sampling of the backbone ϕ, ψ and side-chain χ_1 and χ_2 dihedral angles, *J. Chem. Theory Comput.*, **8**: 3257–3273.
48. JB Klauda, RM Venable, JA Freites, JW O'Connor, DJ Tobias, C

622 Mondragon-Ramirez, et al., 2010, Update of the CHARMM all-atom additive force
623 field for lipids: Validation on six lipid types, *J. Phys. Chem. B*, **114**: 7830–7843.
624 49. Y Komuro, S Re, C Kobayashi, E Muneyuki, and Y Sugita, 2014, CHARMM
625 force-fields with modified polyphosphate parameters allow stable simulation of the
626 ATP-bound structure of Ca^{2+}-ATPase, *J. Chem. Theory Comput.*, **10**: 4133–4142.
627 50. O Allner, L Nilsson, and A Villa, 2012, Magnesium ion-water coordination and
628 exchange in biomolecular simulations, *J. Chem. Theory Comput.*, **8**: 1493–1502.
629 51. HC Andersen, 1983, RATTLE: A "velocity" version of the SHAKE algorithm for
630 molecular dynamics calculations, *J. Comput. Phys.*, **52**: 24–34.
631 52. S Miyamoto and PA Kollman, 1992, SETTLE: An analytical version of the SHAKE
632 and RATTLE algorithm for rigid water models, *J. Comput. Chem.*, **13**: 952–962.
633 53. G Bussi, D Donadio, and M Parrinello, 2007, Canonical sampling through velocity
634 rescaling, *J. Chem. Phys.*, **126**: 014101.
635 54. G Bussi, T Zykova-Timan, and M Parrinello, 2009, Isothermal-isobaric molecular
636 dynamics using stochastic velocity rescaling, *J. Chem. Phys.*, **130**: 074101.
637 55. T Darden, D York, L Pedersen, 1993, Particle mesh Ewald: An N•log(N) method
638 for Ewald sums in large systems, *J. Chem. Phys.*, **98**: 10089–10092.
639 56. PJ Steinbach and BR Brooks, 1994, New Spherical-cutoff methods for long-range
640 forces in macromolecular simulation, *J. Comput. Chem.*, **15**: 667–683.
641 57. EO Oloo and DP Tieleman, 2004, Conformational transitions induced by the
642 binding of MgATP ot the vitamin B_{12} ATP-binding cassette (ABC) transporter
643 BtuCD, *J. Biol. Chem.*, **279**: 45013–45019.
644 58. C Kandt and DP Tieleman, 2010, Holo-BtuF stabilizes the open conformation of
645 the vitamin B12 ABC transporter BtuCD, *Proteins*, **78**: 738–753.
646 59. C Pan, J Weng, and W Wang, 2016, Conformational dynamics and protein–
647 substrate interaction of ABC transporter BtuCD at the occluded state revealed by
648 molecular dynamics simulations, *Biochemistry*, **55**: 6897–6907.
649 60. G Tombline, L Bartholomew, K Gimi, GA Tyndall, and AE Senior, 2004, Synergy
650 between conserved ABC signature Ser residues in P-glycoprotein catalysis. *J. Biol.*
651 *Chem.*, **279**: 5363–5373.
652 61. ML Oldham and J Chen, 2011, Crystal structure of the maltose transporter in the
653 pretranslocation intermediate state, *Science*, **332**: 1202–1205.
654 62. A Yukawa, R Iino, R Watanabe, S Hayashi, and H Noji, 2015, Key chemical factors

655 of arginine finger catalysis of F1-ATPase clarified by an unnatural amino acid
656 mutation, *Biochemistry*, **54**: 472–480.
657 63. AJ Rice, FJD Alvarez, KM Schultz, CS Klug, AL Davidson, and HW Pinkett, 2013,
658 EPR Spectroscopy of $MolB_2C_2$-A reveals mechanism of transport for a bacterial
659 type II molybdate importer, *J. Biol. Chem.*, **288**: 21228–21235.
660 64. HW Pinkett, AT Lee, P Lum, KP Locher, and DC Rees, 2007, An inward-facing
661 conformation of a putative metal-chelate-type ABC transporter, *Science*, **315**: 373–
662 377.
663 65. RN Hvorup, BA Goetz, M Niederer, K Hollenstein, E Perozo, and KP Locher, 2007,
664 Asymmetry in the structure of the ABC transporter-binding protein complex
665 BtuCD-BtuF, *Science*, **317**: 1387–1390.
666 66. H Qasem-Abdullah, M Perach, N Livnat-Levanon, and O Lewinson, 2017, ATP
667 binding and hydrolysis disrupt the high-affinity interaction between the heme ABC
668 transporter HmuUV and its cognate substrate-binding protein, *J. Biol. Chem.*, **292**:
669 14617–14624.
670 67. W Humphrey, A Dalke, and K Schulten, 1996, VMD: visual molecular dynamics, *J.*
671 *Mol. Graphics.*, **14**: 33–38.
672 68. The PyMOL Molecular Graphics System, Version 1.7 Schrödinger, LLC.
673

Figures

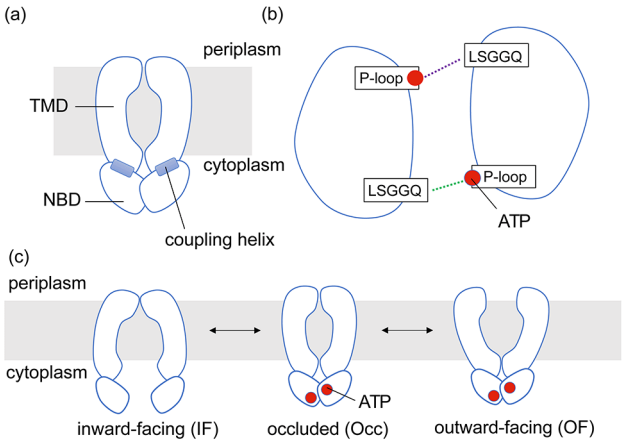

Figure 1. Architecture and alternating access mechanism of ABC transporter. (a) A shared architecture of ABC transporter. Transmembrane domains (TMDs) are embedded in the biological membrane, whereas nucleotide-binding domains (NBDs) are exposed to the cytoplasm. They are physically connected by the coupling helices. (b) Dimerization interface of NBDs as seen from the periplasmic side. They dimerize upon binding of ATP to the P-loop in a head-to-tail fashion, where the P-loop of one monomer binds to the LSGG[E/Q] motif of the opposing monomer. (c) An alternating access mechanism of ABC transporter. The conformational transition from the inward-facing (IF) to the outward-facing (OF) form involves the binding of ATP to the NBDs and the formation of the occluded (Occ) state.

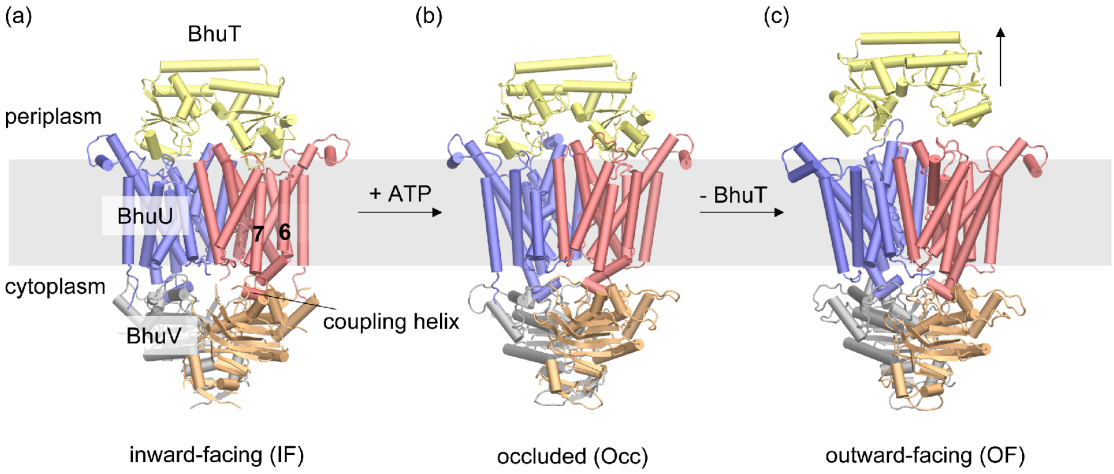

Figure 2. Structures of heme importer BhuUV-T. (a) Crystal structure of BhuUV-T complex (PDB 5B58) in the inward-facing conformation. Transmembrane domains (TMDs, dimer of BhuU) are shown in blue or red. Nucleotide-binding domains (NBDs, dimer of BhuV) are shown in gray or orange. Periplasmic binding domain (PBP, BhuT) is shown in yellow. (b,c) Alternate conformations of BhuUV-T predicted in this study. (b) The occluded and (c) the outward-facing conformations.

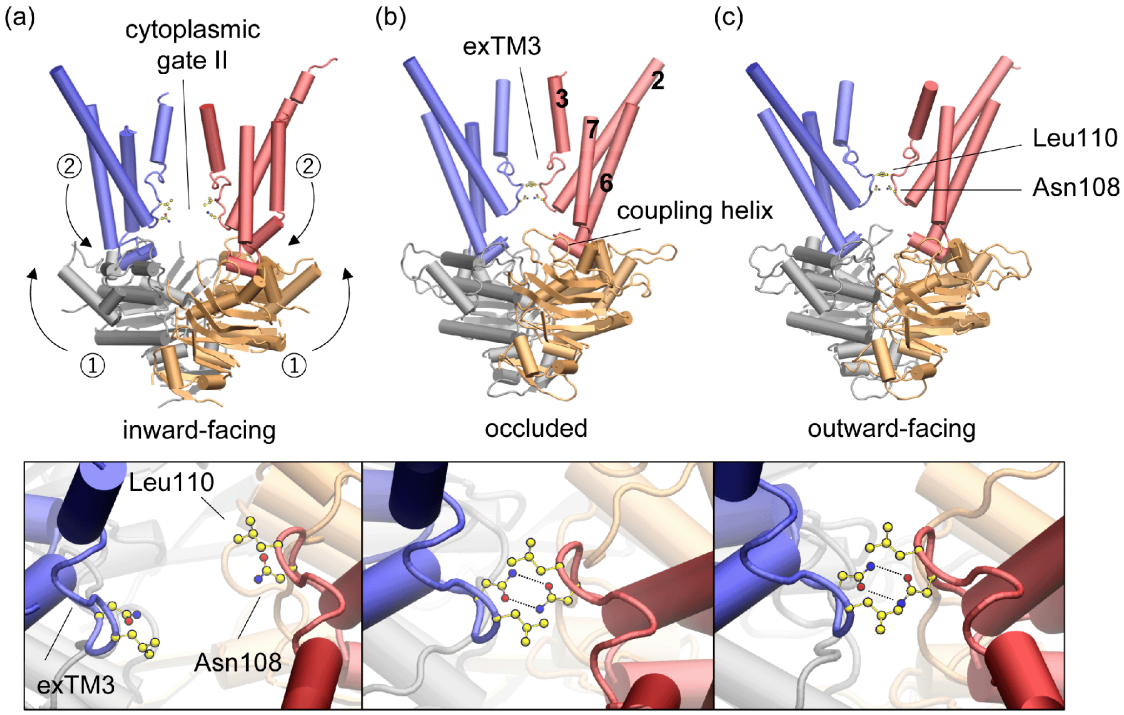

Figure 3. Closure of the cytoplasmic gate II coupled to NBD dimerization. The cytoplasmic gate is open in the inward-facing (IF) conformation (a), while it is closed in the occluded (Occ) (b) and the outward-facing (OF) (c) conformations. The upper panels show the transporter from the membrane space and the lower ones from the periplasmic space. Only TM2–3 and 6–7 are shown for the TMDs. Carbon, nitrogen, and oxygen atoms are in yellow, blue, and red, respectively.

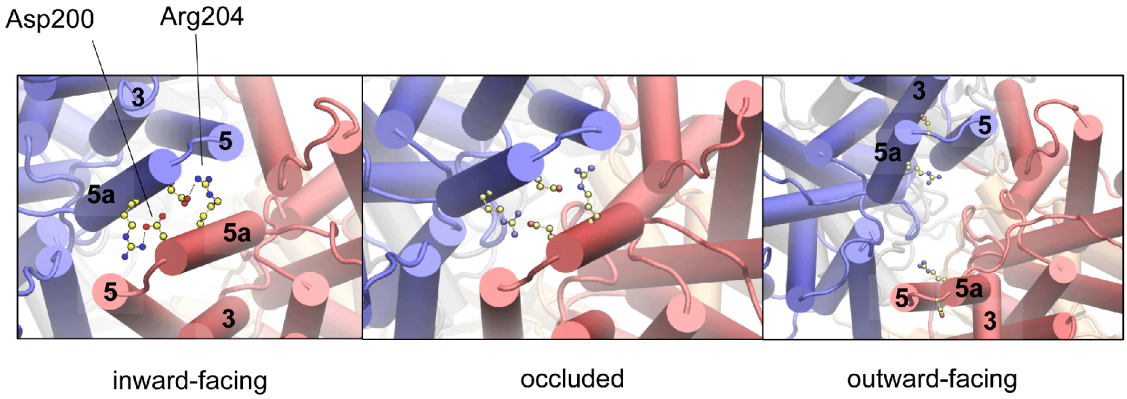

Figure 4. Opening of the periplasmic gate upon the binding of ATP. The panels show the transporter from the periplasm space. In the inward-facing (IF) state (left, PDB 5B58), the periplasmic gate is sealed by TM5 and 5a of opposing monomers. The inter-domain salt bridges between Asp200 and Arg204 stabilize the dimer interface. The situation is not changed in the predicted occluded (Occ) state (middle), while in the predicted outward-facing (OF) state (right), the gate is wide open due to the large tilt of the TM helices.

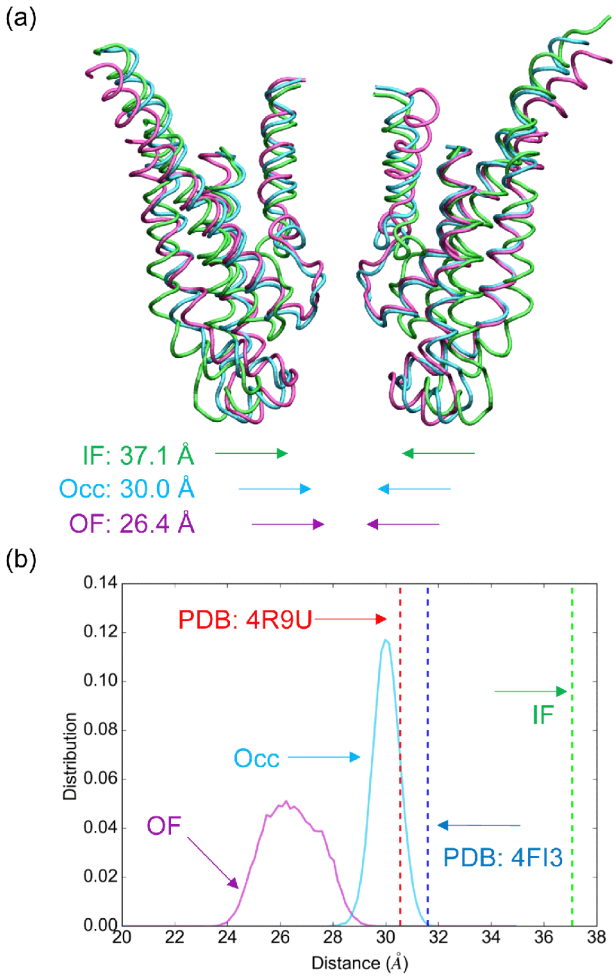

Figure 5. Comparison of the distance between the coupling helices of type II ABC importers in different conformational states. (a) The predicted OF (magenta) and Occ (sky blue) average structures along the last 500-ns equilibrium MD simulations are superimposed on the IF crystal structure (green). Only TM2–3 and TM6–7 of the TMDs are shown. Distance between the coupling helices (CHs) for each structure is denoted at the bottom. (b) Distribution of distance between the CHs in the last 500-ns equilibrium MD simulation for each conformation.

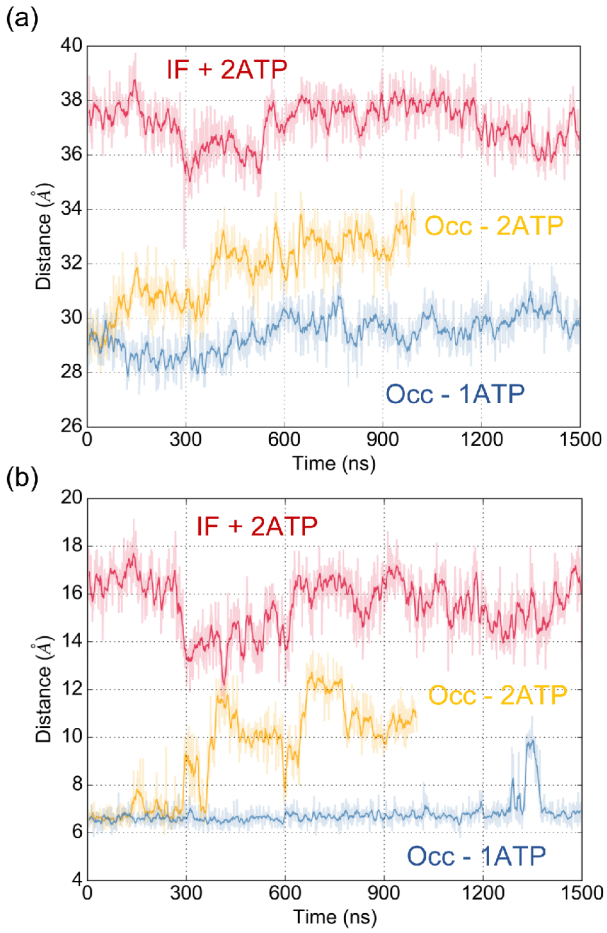

Figure 6. Structural changes in the equilibrium MD simulations. (a,b) Temporal changes of distance between (a) the coupling helices and (b) Leu110 of opposing monomers during the MD-IF-2ATP (IF + 2ATP), MD-apo-Occ (Occ – 2ATP), and MD-Occ-1ATP (Occ – 1 ATP) trajectories.

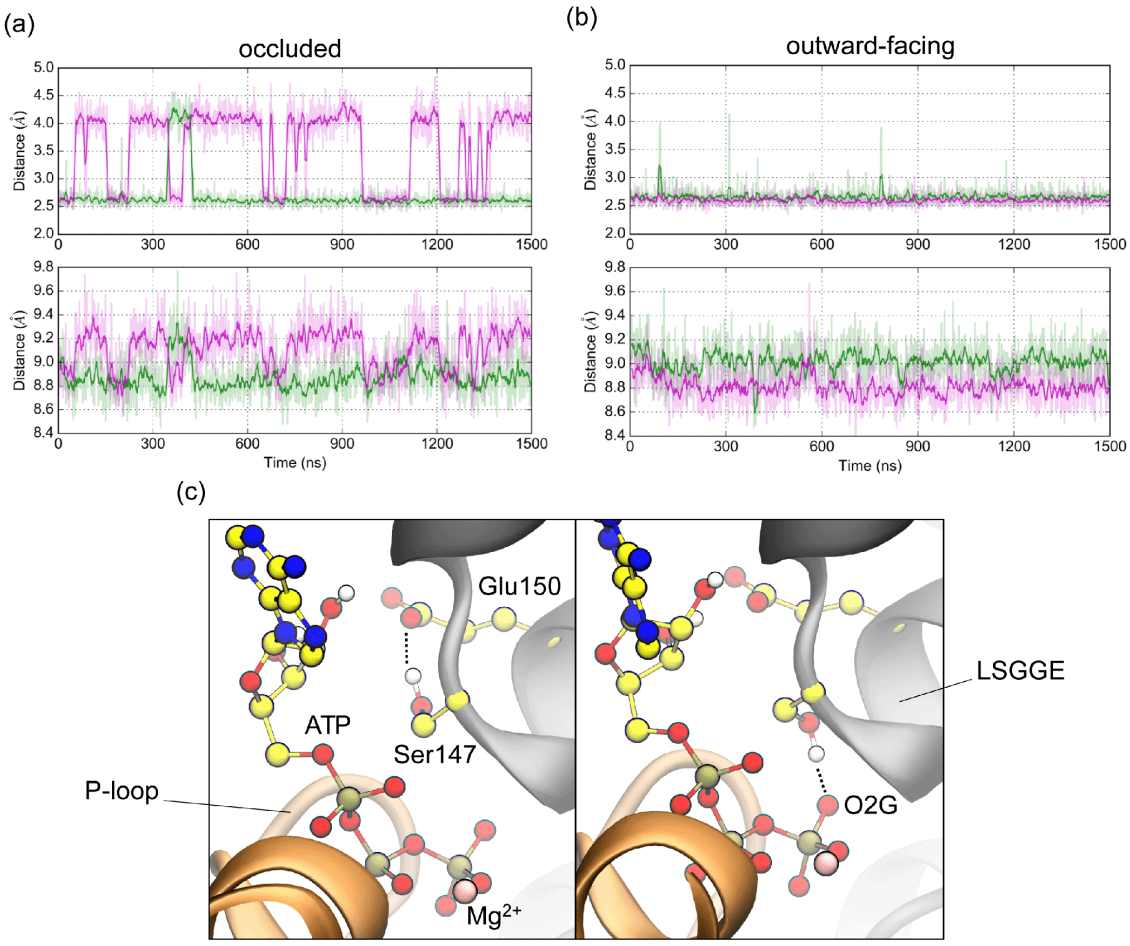

Figure 7. Alternate configurations of Ser147. (a,b) The upper panel shows the distance between OG atom of Ser147 and O2G atom of ATP and the lower one shows the distance between P-loop and LSGGE for the occluded state (a) and the outward-facing states (b). Here, the two nucleotide-binding sites (NBSs) are designated as NBS1 and NBS2, and the results for NBS1 and NBS2 are indicated by magenta and green lines, respectively. (c) Two possible orientations adopted by the side chain of Ser147 observed in the simulation of the occluded state.

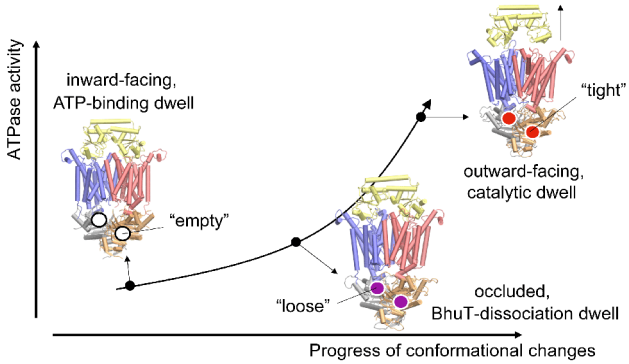

Figure 8. Proposed chemo-mechanical coupling model. The horizontal axis describes progress of conformational changes (e.g. distance between coupling helices), whereas the vertical axis indicates the ATPase activity of the protein. In this model, the progress of conformational changes is coupled to the ATPase activity of the protein (the curved arrow) so that as the conformation transition proceeds from the inward-facing (IF) state to the outward-facing (OF) one, the ATPase activity gradually increases.